CrystEngComm

PAPER

View Article Online
View Journal | View Issue

Cite this: *CrystEngComm*, 2017, **19**, 4519

Amino acid-assisted controlling the shapes of rutile, brookite for enhanced photocatalytic CO_2 reduction†

Quang Duc Truong, *[a] Thi Hang Le[a] and Huu Thu Hoa[b]

Received 24th March 2017,
Accepted 10th July 2017

DOI: 10.1039/c7ce00566k

rsc.li/crystengcomm

TiO_2 nanoparticles with a controlled crystalline phase, size, shape and surface structure have been synthesized by a facile hydrothermal method using a water-soluble titanium complex and amino acid as the structure-directing and shape-controlling agents. The titania phases of rutile or brookite can be easily tuned by using different amino acid additives. Rutile nanorods with a high aspect ratio have been obtained in the presence of glutamic acid. Small nano-sized and well-faceted brookite can be synthesized using lysine as a pH-adjusting and shape-controlling agent. Amino acids play crucial roles in determining the crystalline phase as well as size and shape of the synthesized nanoparticles. The synthesized TiO_2 rutile and brookite with different shapes have been evaluated for photocatalytic activity by means of the reduction of carbon dioxide to methanol. The investigation results reveal that the methanol yield on rutile and brookite strongly depends on the crystalline phase, size, shape and surface structure of the synthesized nanocrystals. Among the rutile nanocrystals, the photocatalytic activity increases with an increasing percentage of the {111} surface. Brookite with exposed {210} facets exhibits a notable photocatalytic activity for CO_2 reduction presumably due to its specific surface structure with a spatial separation of reductive and oxidative sites. Our studies demonstrate the abilities of shape-control and facet-selectivity in determining photocatalytic activity, representing a critical step forward in the designing of high performance nanostructures for the reduction of CO_2.

1. Introduction

Recently, climate change and energy shortages have raised special attention worldwide and have accelerated the development of environmental protection and renewable energy technologies. The development of advanced catalysts with their intriguing properties and wide applications in the simultaneous reduction of carbon dioxide and production of a renewable energy source, therefore, has gained increasing attention. Although Honda and Fujishima introduced the reduction of CO_2 using a TiO_2 photocatalyst in the late1970s,[1] progress in this field has been very slow compared to that in the development of catalyst for water splitting. Because methanol is one of the most promising alternative fuels, the photoreduction of CO_2 into methanol offers an intriguing opportunity to achieve solar fuels.[2,3] For instance, considerable efforts have been devoted to explore the photocatalytic reduction of CO_2 into methanol.[4–9] Very recently, some advances have been achieved in the selective reduction of CO_2 on various catalysts such as Cu/ZnO, In_2O_3, and TiO_2 materials.[8–10]

Titanium dioxide is one of the most promising candidates for photocatalytic reactions, such as CO_2 reduction or water splitting, owing to its powerful oxidation properties, availability, efficiency and long-term stability.[10–12] The synthesis of titania nanocrystals with a controlled size and shape, and exposed reactive facets, thus, has been investigated towards harvesting energy and reducing CO_2.[10–12] It was reported that the photochemical properties of interfacial reactions in a heterogeneous catalytic system will be dominated by the surface properties of the catalysts.[13] Therefore, controlling the shape and surface structure is of critical importance for an enhanced performance in photocatalytic reaction, especially for the photocatalytic reduction of CO_2.[12] Up to now, efforts have been made on the investigation of anatase nanocrystals with different shapes and their photocatalytic reduction of CO_2.[14,15] The shape-controlled synthesis and photocatalytic CO_2 reduction activity of rutile and brookite are less studied. This may be due to the fact that the controlled synthesis of rutile and brookite is thermodynamically difficult.[16]

Recently, we proposed a novel route for controlling the crystalline structure, size, shape and organized features of

[a] *Institute of Multidisciplinary Research for Advanced Materials, Tohoku University, Sendai 980-8577, Japan. E-mail: tqduc@tagen.tohoku.ac.jp*
[b] *Faculty of Chemistry, VNU University of Science, Vietnam National University, 19 Le Thanh To1ng, Hanoi 100000, Vietnam*

† Electronic supplementary information (ESI) available. See DOI: 10.1039/c7ce00566k

nanostructures using water-soluble compounds which are formed by the coordination of small organic molecules to metals in stable complex structures.[17–20] The nucleation and assembly of the desired nanostructures can be readily tuned by a sophisticated bottom-up approach based on the nature of the coordination complex. For example, a new series of titanium precursors has been developed, namely water-soluble titanium complexes, for the selective synthesis and morphological control of TiO_2 polymorphs.[16–19] In a previous report, we used picolinic acid for the synthesis of rutile with exposed high-index facets which showed an enhanced photocatalytic reduction of CO_2.[20] We now report the controlled fabrication of TiO_2 nanocrystals with controlled phases, shapes and exposed facets using amino acid as the structure-directing and shape-controlling agent. From the structure viewpoint, amino acid with amine and carboxyl groups can act as a rich coordination ligand providing selective adsorption and metal ion complexation, which are crucial for a morphological control synthesis.[21] Furthermore, crystal growth induced by the oriented attachment *via* van der Waals interaction and hydrogen bonding with the aid of organic molecules has proved to be an effective route for controlling particle assembly.[22] Herein, rutile and brookite with a tunable shape have been selectively synthesized using different amino acid additives. Chemical and physical properties of the obtained nanocrystals and their photocatalytic activity by means of the reduction of CO_2 were intensively studied. The effects of the crystalline structure and shape of the synthesized particles on the methanol yields were also investigated in detail.

2. Experimental section

2.1. Synthesis of TiO_2

TiO_2 was synthesized according to a previously reported method with an amino acid additive.[16–20] Briefly, a yellowish transparent peroxo-titanic acid solution was prepared by the addition of an ammonia solution (2 cm^3, 28%, Kanto Chemicals Co., Inc.) and a hydrogen peroxide solution (10 cm^3, 30%, Kanto Chemicals Co., Inc.) to titanium metal powder (2 mmol, Wako Pure Chemical Industries Ltd.). Glycolic acid (3 mmol, Kanto Chemicals Co., Inc.) was added to the yellowish solution of peroxo-titanic acid, as a result of which the solution color changed from yellowish to pale red. Heat treatment at 353 K was carried out to remove excess ammonia and hydrogen peroxide. Finally, a stable titanium complex solution of a yellow-red color was obtained. Then, amino acid (Table S1,† 2 mmol, Kanto Chemicals Co., Inc.) was added to the complex solution. The solution of the complex was diluted to 20 cm^3 using distilled water, placed in a Teflon-lined reactor and sealed in stainless steel autoclaves. The autoclave was heated at 473 K for 24 h for the hydrothermal treatment of the complexes. After that, the autoclave was allowed to cool down to room temperature. The resultant powders were separated by centrifugation and washed with distilled water until the obtained solution had a neutral pH. All the catalyst samples dispersed again in distilled water and were irradiated by UV light from a high-pressure mercury lamp to eliminate organic residues on the TiO_2 surface prior to the photocatalytic test. Finally, the obtained specimen was dried at 353 K for 1 day.

2.2. Photodeposition of Pt co-catalyst on TiO_2 particles

Pt nanoparticles as cocatalysts were deposited on TiO_2 by a photodeposition method in a closed system. Typically, a suspension containing TiO_2 (100 mg) and 5 μmol H_2PtCl_6 in methanol solution (10 mL/40 mL) was irradiated with light from a 500 W Xe lamp for 1 h with stirring to obtain 1 wt% Pt/TiO_2. Generally, it is accepted that a limited amount of H_2PtCl_6 will be deposited completely on the catalyst upon the light irradiation. The obtained precipitate was separated by centrifugation, washed repeatedly with fresh water, and dried in air at room-temperature overnight. Finally, the obtained powder was dried at 60 °C for 12 h, yielding Pt/TiO_2.

2.3. Characterization of the synthesized particles

The crystalline phase of the samples was characterized using powder X-ray diffraction (XRD; Rigaku RINV-2200, 40 kV and 30 mA) with CuKα radiation (λ = 1.5406 Å). Data were collected in the 2θ–θ scanning mode with a scan speed of 4° min^{-1} and a step size of 0.02°. The morphology of the particles was observed using a field-emission scanning electron microscope (FE-SEM, Hitachi S-4800) at an accelerating voltage of 5 kV. Transmission electron microscopy (TEM Hitachi H-7650, 100 kV) and High Resolution TEM (HR-TEM, Hitachi HF-2000) were conducted. Nanocrystals were dispersed in ethanol and then dropped onto a Cu microgrid coated with a holey carbon film, followed by vacuum evaporation at 60 °C. IR spectra were recorded with a Jasco spectrometer within the range of 400–4000 cm^{-1}. Samples in the solid state were measured in KBr matrix pellets obtained with a hydraulic press under 40 kN pressure. DRS spectra of the solid samples were evaluated in the range of 200–800 nm with a spectrophotometer instrument (Shimadzu, UV 2450). N_2 adsorption and desorption isotherms were measured at 77 K (Micromeritics ASAP 2010) to yield the Brunauer–Emmett–Teller (BET) specific surface area.

2.4. Photocatalytic reduction of CO_2

The photocatalytic reduction of CO_2 was carried out in an aqueous system under UV-vis irradiation according to our previous reports.[23,24] In brief, 50 mg of catalyst was dispersed in 30 ml of distilled water containing sodium bicarbonate ($NaHCO_3$, 0.1 M). Ultrahigh purity CO_2 (99.99%) was pursed continuously into the reactor at a rate of 0.1 L min^{-1} for 0.5 h to remove oxygen in the water, and saturate carbon dioxide in the solution. The solution was prepared in a 30 cm × 15 cm × 5 cm reactor. The reaction system was initially tested to afford the optimal catalyst concentration of 1.65 g dm^{-3}. A fixed catalyst concentration was used in all the experiments, aiming to

eliminate uncertainties associated with light reflection and reactor geometry. The solution was stood in the dark for 30 min until reaching adsorption–desorption equilibrium. The solution temperature was kept constant by a water bath. UV-vis light irradiation was provided by a 500 W high-pressure Xe lamp placed above the reactor. A Pyrex glass was placed on top of the reactor to cut off light with wavelengths $\lambda < 300$ nm. The photocatalytic reaction was continued for up to 9 h and at every 1 h interval, the solution in the reactor was sampled. The sample solution was centrifuged and analyzed by GC-FID for CH_3OH with a 2 m Porapak Q column. The rate of CH_3OH evolution was defined as the total amount of evolved CH_3OH divided by the reaction time.

The photoreduction of CO_2 by various catalysts has been extensively studied.[1–10,25,26] The following reaction was proposed for the selective production of CH_3OH:

$$2CO_2 + 4H_2O \rightarrow 2CH_3OH + 3O_2 \quad (1)$$

Prior to the photocatalytic reaction, the TiO_2 catalyst was dispersed in distilled water and irradiated by UV light from a high-pressure mercury lamp for 5 h, aiming to remove any organic residues on the TiO_2 surface. We carried out control experiments in the dark first and no CH_3OH was detected for all the tested catalysts. Similarly, no CH_3OH was detected for control experiments under light irradiation but without a catalyst. Preliminarily results from these control experiments indicate that both light irradiation and catalysts are indispensable for CO_2 photoreduction into CH_3OH.

3. Results and discussion

3.1. Structure and morphology of TiO_2

Hydrothermal treatment of the titanium–glycolate complex yielded single-phase rutile and brookite at pH 6.0 and 10.0, respectively (Fig. S1†).[16] XRD patterns of the particles obtained by hydrothermal treatment of the water-soluble titanium glycolate complex with different amino acid are shown in Fig. 1. The XRD patterns indicate that all the samples consist of crystalline titanium oxide without impurity. Anatase is crystalline phase obtained by the treatment of the complex with Asp and Tyr, while a single-phased rutile was formed in the presence of Ala, Gly, Pro, Glu, Ser, Thr, Cys, or Met. Interestingly, the addition of Lys or Arg to the complex solution resulted in the production of brookite as a major phase (70–80% of brookite) (Fig. 1g and h). The existence of brookite is clearly evident from the presence of a characteristic peak at 2θ = 30.81° where no overlapping by those of anatase or rutile is present (Fig. S1†). A mixture phase of rutile/brookite was obtained in the case of using His. To obtain single phase of brookite, an increasing amount of Lys (3 mmol) was further introduced into the complex solution before the hydrothermal treatment. Fig. S1q† reveals that single-phased brookite has been synthesized in the presence of Lys. We used the method proposed by Banfield *et al.*[27] to estimate the phase composition of rutile (R%) and brookite (B%) of a sample synthesized using His as follows:

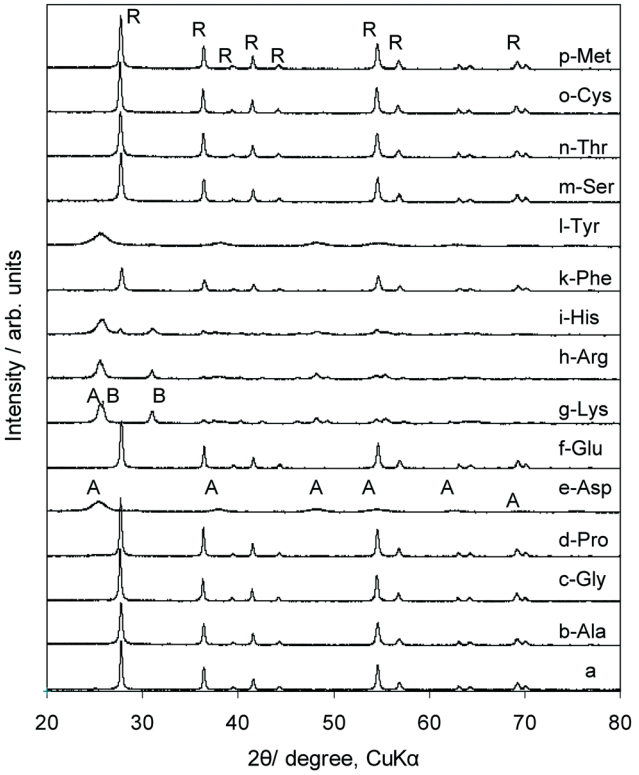

Fig. 1 XRD patterns of the particles synthesized by hydrothermal treatment of titanium–glycolate in the presence of different amino acids. A: Anatase, B: brookite, R: rutile.

$$B\% = 100I_B/(I_B + 2.721I_R)$$
$$R\% = 100 \times 2.721I_R/(I_B + 2.721I_R) \quad (2)$$

where I_R and I_B represent the XRD peak intensity of the rutile (110) and brookite (121), respectively.[27] Similarly, the phase composition of anatase (A%) and brookite (B%) of the sample synthesized using Lys or Arg could also be estimated.[27] The polymorph composition of all the samples is listed in Table S1.† Moreover, based on the XRD patterns and the Scherrer equation, the crystallite size of different phases could also be calculated, as given in Table S1.† The crystallite size of rutile synthesized in the presence of amino acids is readily reduced with respect to that of rutile particles obtained without amino acid. A similar tendency is also observed for brookite-type particles.

The crystalline structures were also confirmed using Raman spectroscopy. As shown in Fig. 2, anatase obtained with Asp as the additive has characteristic bands at 400 cm^{-1} (optical mode: B1g), 522 cm^{-1} (A1g) and 642 cm^{-1} (Eg(3)), while rutile prepared using Glu (hereafter denoted as R_{Glu}) shows two peaks at 448 cm^{-1} (Eg) and 612 cm^{-1} (A1g). Generally, Raman spectroscopy is an efficient characterization method to clarify the appearance of brookite phases.[19,28] As shown in

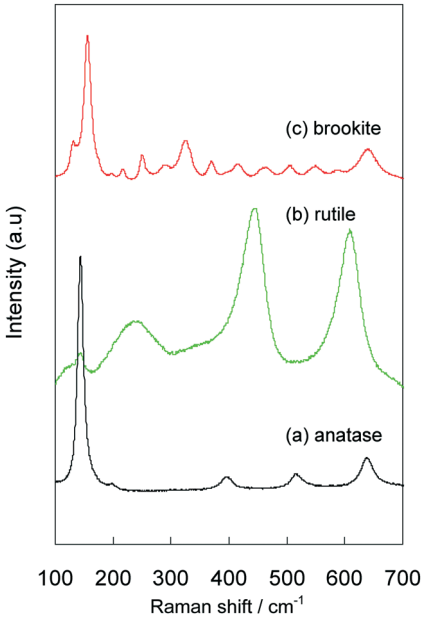

Fig. 2 Raman spectra of the particles synthesized using: (a) Asp (anatase), (b) Glu (rutile), and (c) Lys (100% brookite).

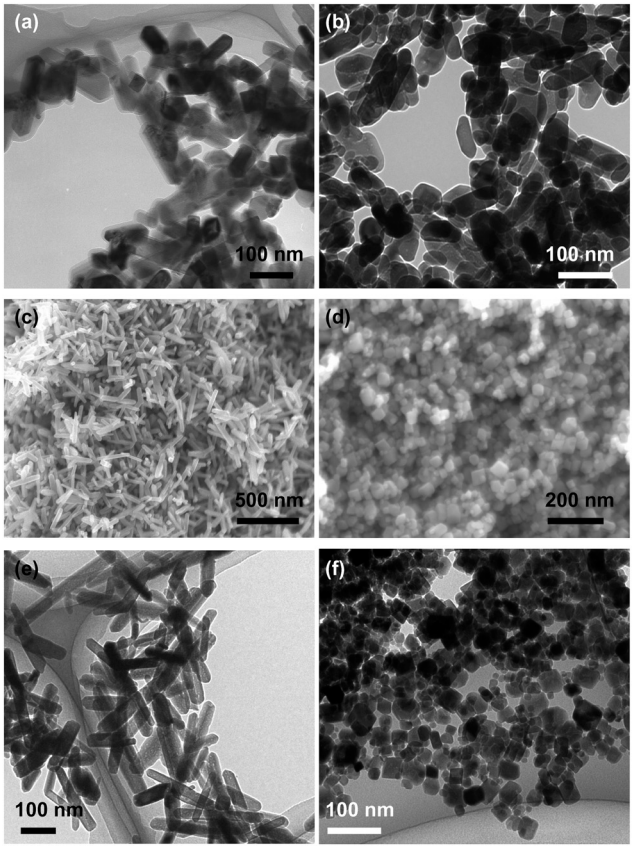

Fig. 3 TEM images of the synthesized particles from titanium–glycolate at pH (a) 6.0, rutile (b) 10.0, brookite. SEM (c and d) and TEM (e and f) images of the synthesized particles using (c and e) Glu, rutile and (d and f) Lys, 100% brookite.

Fig. 2c, the single-phased brookite synthesized with Lys (hereafter denoted as B_{Lys}) has the Raman shift peaks of brookite with one strong Raman peak at 156 cm^{-1} (A1g) and 13 weak peaks at *ca.* 126, 197, 215, 245, 287, 320, 365, 414, 460, 502, 548, 589, and 637 cm^{-1}.[19] These shift peaks indicate that brookite is the only phase present in the synthesized particles due to the absence of shift peaks inherent in anatase (400 cm^{-1} and 522 cm^{-1}) and rutile (448 cm^{-1} and 612 cm^{-1}).

The effect of amino acid on the size and shape of the obtained particles in the present study was also investigated by SEM and TEM. As shown in Fig. 3 and Fig. S2–S4,† all the samples consist of nano-sized particles. The synthesized rutile and brookite in the absence of amino acid are composed of mainly nanorod particles with low aspect ratios (Fig. 3a and b). Rutile obtained by hydrothermal treatment in the presence of Glu (R_{Glu}) comprises 20–150 nm rod-like particles which have a much higher aspect ratio compared to that of rutile obtained without additive (Fig. 3c and e). Fig. S4† shows electron microscopic images of the anatase–brookite particles obtained by hydrothermal treatment of the complex with Lys. The synthesized anatase–brookite particles disperse uniformly and display a mainly spherical morphology with an average diameter of 10 nm. The single-phased brookite-type particles synthesized in the presence of Lys (B_{Lys}) are composed of well-faceted nanocrystals of different shapes with sizes in the range of 10–30 nm (Fig. 3d and f). These brookite nanoparticles are smaller than the usual size of brookite reported in a previous study.[16]

High-resolution TEM analysis is performed to examine the detailed structure of rutile and brookite. The HRTEM images of rutile and R_{Glu} are shown in Fig. 4a and c. The selected-area electron diffraction pattern in Fig. 4b taken from the branch of rutile can be indexed to the [1–10] zone axis of single-crystal tetragonal TiO_2. A HRTEM image of a nanorod branch of R_{Glu} indicates the growth of the rutile along the [001] direction (Fig. 4d). The exposed side surface and the end of the nanorod are attributed to {110} and {111} facet, respectively. The HRTEM image of B_{Lys} is present in Fig. 4e. The crystallographic structure is identified as brookite TiO_2 by characteristic spacing and angles of the lattice fringes. The B_{Lys} particle is imaged along the $[-12-1]_B$ zone axis, and it is bound by $(210)_B$, with a lattice spacing of 0.35 nm; $(111)_B$, 0.35 nm; and $(-110)_B$, 0.45 nm. The exposed surface facets could not be simply confirmed by HRTEM, so further investigation on SAED and STEM image is needed.

3.2. Effect of amino acid on the shape of rutile and brookite

On the basis of the above results, it is clear that amino acids play a critical role in controlling the crystalline structure and shape of TiO_2. As demonstrated previously, pH is a crucial factor in determining the crystalline phase synthesized from a titanium-complex.[16] Amino acid is also a pH-adjusting agent through its dissociation in an aqueous solution. Thus, anatase, rutile, and brookite are, respectively, obtained in acidic, neutral, and basic solutions of Asp, (Ala, Gly, Pro, Phe, Ser, Thr, Cys, Met) and (Lys, Arg, His), respectively. While pH

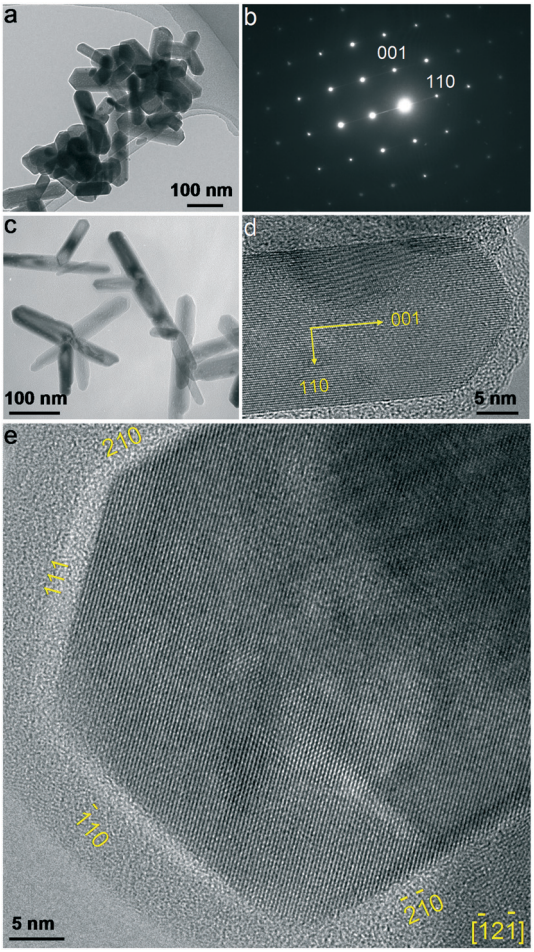

Fig. 4 TEM images of the synthesized particles from titanium–glycolate at pH (a) 6.0, rutile. (b) SAED pattern of rutile branch in (a). (c) TEM image of the synthesized particles using Glu, rutile. (d) HRTEM image of the rutile nanorod in (c). (e) HRTEM image of the synthesized particles using Lys, single-phased brookite.

is crucial in almost all cases, it is not so for Glu and Tyr. Therefore, another factor should be taken into account, namely the capping effect, in which the adsorption of amino acid on the particle interface changes the crystal growth habit of titania, resulting in the formation of different phases and shapes.

It is well-known that a capping strategy is particularly efficient to control the growth of nanocrystals in desired surface structures or shapes.[19,20] The additives may provide a chemical bond to the dangling atom on the particle surface, and thus reduce the interface tension and stabilize the adsorbed surfaces. The interface tension of different facets of anatase nanocrystals can be altered by selective adsorption of amino acid additives such as Glu or Asp.[21] As a result of this, high energy {001} facets can be gradually eliminated during the crystal growth, leading to the growth of a high aspect ratio ellipsoid nanocrystals.[21] It has been found that amino acids such as Glu may selectively adsorb on the {101} facets of anatase, resulting in the formation of rod-like nanocrystals with preferential growth in the [001] direction.[21] On the other hand, the possible adsorption configuration of the rutile {110} surface is similar to that of the anatase {101} surface. Thus, it is reasonable that Glu is also selectively adsorbed on the {110} facets of rutile, favoring the growth of the rutile nanorod in the [001] direction with a high aspect ratio (Fig. 5a).

In order to verify the above discussion, FTIR spectra of the as-prepared TiO_2 samples were investigated. Fig. S5a† shows the FTIR spectra of glutamic acid functionalized TiO_2 (R_{Glu}) in comparison with those of glutamic acid and a TiO_2 commercial product (P25). According to the spectra, the peaks around 1680 cm^{-1} can be assigned to the stretching vibrations of the hydroxyl group surface of titanium oxide. Besides that, the peaks at 1405 cm^{-1} and 1540 cm^{-1} are attributed to the asymmetric and symmetric stretching vibrations of $-COO^-$, which can be observed in R_{Glu}. The $\nu_S(COO^-)$ stretching frequency observed in the FTIR of the synthesized particles indicates that the carboxyl group is deprotonated due to the chelation to surface titanium ions. Furthermore, the presence of a band at around 1710 cm^{-1} corresponding to the stretching vibration of COOH group implies that one of the carboxyl groups has not been deprotonated. And the peak at 1100 cm^{-1} is attributed to the stretching vibrations of C–N from glutamic acid. This result further indicated that glutamic acid molecules were adsorbed on the surface of TiO_2 and may play an important role in the formation of the high aspect ratio rod-like nanostructures.

The formation of nano-sized well-faceted brookite particles can also be explained by the capping effect. Lys may

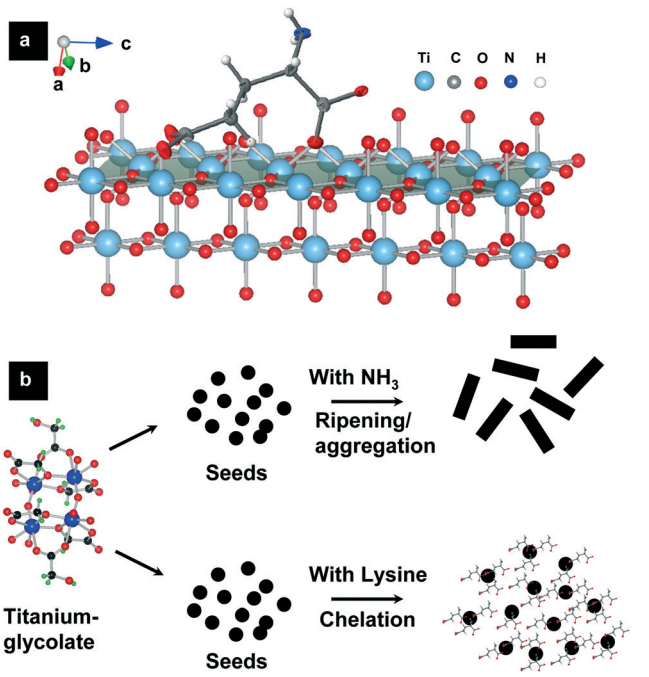

Fig. 5 (a) A possible model of glutamic acid adsorption on the {110} face of rutile. Surface hydroxyl groups are omitted for clarify. (b) Schematic representation of the formation mechanism of brookite with different morphologies: (top) a growth process in the absence of amino acid; (bottom) in the presence of amino acid.

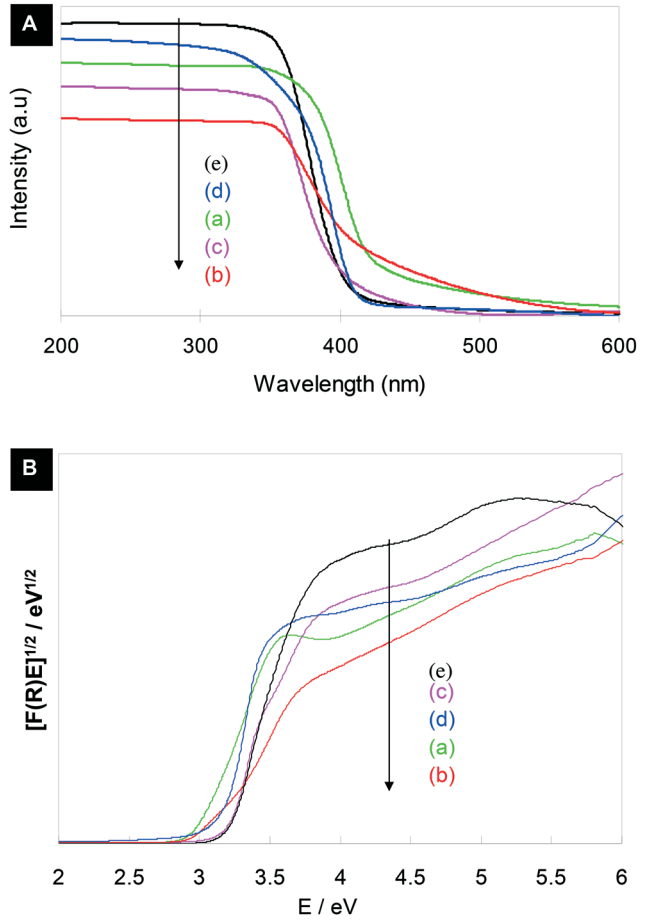

Fig. 6 (A) UV-vis DRS spectra of the synthesized particles (a) rutile, (b) R_{Glu}, (c) brookite, (d) B_{Lys}, and (e) P25. (B) Plot of the Kubelka–Munk function *versus* the energy of light absorbed.

provide a specific interaction with the brookite surface through its functional groups, and thus restrain the growth of larger crystals (Fig. 5b). It should be mentioned that brookite obtained under the alkaline conditions of ammonia or urea,[29,30] where no capping effect is pronounced, forms very large crystallites of rod-like, snowflake-like or multi-needle shape. In the presence of an additive such as an oleate anion, however, a nano-sized brookite of pseudocubic crystal shape could be grown due to the selective adsorption of the additive on brookite surface.[19] In the present system, the presence of Lys on the surface of brookite is evidenced from the FT-IR analysis as shown in Fig. S5b.† Thus, it can be concluded that Lys with its amine and carboxyl groups may form a complexation with Ti on the particle interface, thus providing the capping effect (Fig. 5b). The selective chelation of Lys on a specific brookite surface may be attributed to the growth of well-faceted nanocrystals as shown in Fig. 3d and f. The study on these selective facets and their growth is under progress.

3.3. UV-vis DRS and band gap energy studies

The optical properties study only refers to rutile and brookite whose photocatalytic activity is discussed later. Diffuse reflectance spectra of the synthesized TiO_2 in comparison with that of Degussa P25 are shown in Fig. 6A. It is obvious that absorption band of the synthesized particles somewhat shifts toward longer wavelengths with respect to that of the commercial product P25. The absorption intensity of the rutile particles dominates that of the P25 or brookite particles. The absorption in the visible-light region increases in the order P25 < brookite < rutile.

In order to gain insight into the optical properties of titania powder, the band gap energies of the synthesized materials were studied in detail. The band gap energies can be determined by plotting the modified Kubelka–Munk function $[F(R)E]^{1/2}$ calculated from the optical absorption spectrum *vs.* the energy of the exciting light (Fig. 6B). The values are given in Table 1. The band gap of brookite synthesized with Lys is at around 3.20 eV, whereas that of rutile is about 3.00 eV.

3.4. Photocatalytic CO_2 reduction

The photocatalytic activities of the synthesized TiO_2 rutile and brookite were evaluated in terms of photocatalytic CO_2 reduction from aqueous solution under UV-vis ($\lambda > 300$ nm) irradiation. The results of the photocatalytic study only refer to rutile and brookite, whose photocatalytic CO_2 reduction were less reported. Table 1 lists the methanol yields, specific BET surface areas and other physical properties of the corresponding samples. The rutile samples include whisker particle $R_{Whisker}$,[18] nanorod R_{Glu} (Fig. 3c and e), rutile (Fig. 3a) and flowerlike particles with exposed high-index facets R_{Flower}.[20] Under the irradiation of light, brookite samples exhibited a higher activity than those of rutile (Fig. 7). The methanol yields on the brookite samples are in range of

Table 1 Chemical and physical properties and H_2 evolution rate on the TiO_2 catalysts

Sample	Cryst. size[a] (nm)	{111} %	Band gap (eV)	BET ($m^2\ g^{-1}$)	CH_3OH μmol g^{-1}	CH_3OH μmol g^{-1} m^{-2}
[b]$R_{Whisker}$	30	5	—	21.0	3.50	0.166
R_{Glu}	23	10	3.0	40.2	3.14	0.078
Rutile	32	30	3.0	28.2	4.63	0.164
[c]R_{Flower}	45	50	—	17.0	5.12	0.30
Brookite	25	—	3.2	28.8	7.08	0.246
B_{Lys}	17	—	3.2	35.7	9.22	0.258

[a] Estimated according to the Scherrer equation: $D_{(hkl)} = (K\lambda)/(\beta \cos\theta)$ where K is the shape factor, λ the wavelength of the Cu Kα radiation, β the full width at half-maximum (fwhm) of the (hkl) peak, and θ the diffraction angle. [b] Ref. 18. [c] Ref. 20.

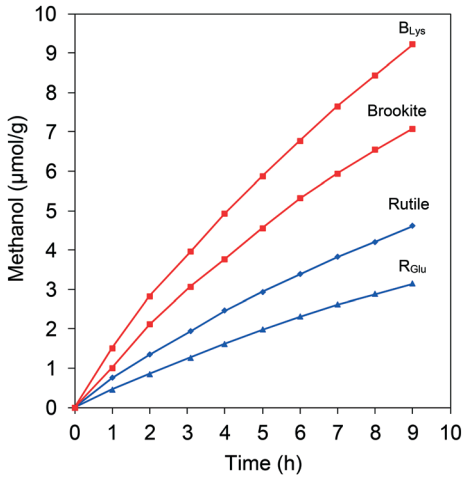

Fig. 7 The time course of methanol evolution on the synthesized particles.

7.08–9.22 μmol g^{-1}, whereas those on rutile are in the range of 3.14–5.12 μmol g^{-1}. R_{Glu} (Fig. 3c and e) showed a lower activity with respect to that of the rutile sample (Fig. 3a). Especially, B_{Lys} (Fig. 3d and f) exhibited a remarkable photoactivity with a methanol yield of 9.22 μmol g^{-1}, that is 1.30 times higher than that on the brookite sample (Fig. 3b).

All the brookite TiO_2 samples exhibited a significantly higher photocatalytic activity than those of the rutile samples, which may be attributed to the nature of crystalline brookite. It has been reported that brookite had a higher photocatalytic activity than those of rutile and anatase.[31] Li *et al.* also reported that the photocatalytic CO_2 reduction activity of a pure brookite suspension was higher than that of pure anatase or rutile, despite the former having a lower surface area.[31] Our results suggest that the brookite-type TiO_2 has a higher activity than that of rutile with the same morphology and specific BET surface area (Table 1). This may be due to the fact that brookite TiO_2 shows the highest reduction ability, from the evaluation of the conduction band potential.[30] The more negative flat band potential is beneficial for CO_2 reduction. We performed the examination of brookite particles after the photocatalytic reaction. The XRD pattern of brookite after the catalytic reaction with light irradiation in Fig. S6† reveals that a phase transformation does not occur.

The different activity of different rutile samples can be understood from their surface structures. All of the rutile TiO_2 with different shapes investigated in the present study were well-crystallized and well-faceted as shown in Fig. 3 and 4, which was, indeed, the result of a slow growth from a stable titanium-complex. In particular, it has been proved that rutile synthesized from titanium–glycolate grows in the [001] direction with the predominant exposure of {110} facets and {111} facets.[18,20] It is observed that the surface area percentage of {111} facets increases in the order $R_{Glu} \approx R_{Whisker} <$ Rutile $< R_{Flower}$, whereas the specific BET surface areas increase in the opposite order (Fig. 8, Table 1). On the basis of the investigation, it is found that that photocatalytic CO_2 reduction activity increases with an increased surface area percentage of {111} facets. For instance, R_{Glu} showed a lower activity compared to that of rutile presumably due to the fact that the former possesses a higher aspect ratio with a smaller percentage of {111} facets. Thus, the methanol yield was found to be strongly dependent on the percentage of the {111} surface.

Ohno *et al.* reported that crystal faces on TiO_2 particles are particularly important to the photocatalytic properties.[32–35] This is due to the fact that oxidation and reduction occur simultaneously on each particle. Because of their different atomic arrangements, the well-developed facets on TiO_2 provide both oxidation and reduction sites, leading to an enhanced efficiency of the electron–hole separation.[32] The selective photodeposition of Pt and PbO_2 indicates that the (110) face provides reductive sites and that the (111) face provides oxidative sites.[33] In this study, it was also observed that Pt particles were deposited on the {110} facets of rutile, as revealed from TEM images of particles after the photodeposition of platinum (Fig. 9a and b). As mentioned above, the photocatalytic activity increases with an increased

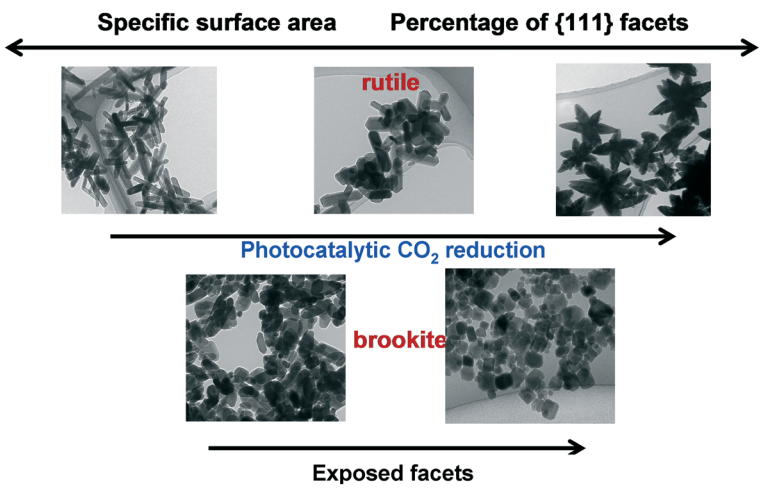

Fig. 8 The correlation between properties and methanol yield on rutile and brookite.

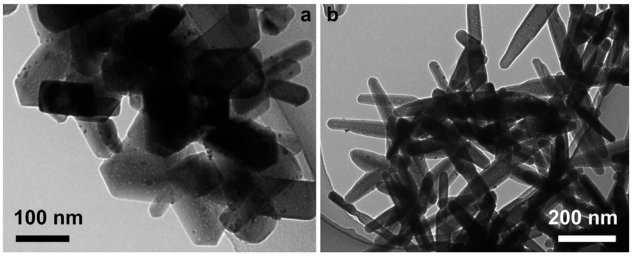

Fig. 9 TEM images of Pt-deposited rutile TiO_2 particles synthesized at pH 6 (a) and rutile whiskers obtained in the presence of glycolic acid (b).[18]

s-

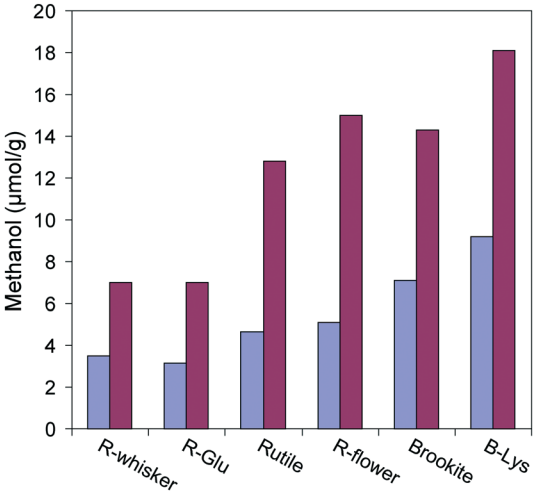

Fig. 10 Methanol yields over bare (violet) and Pt co-catalyst loaded (red) rutile and brookite TiO_2.

urface area percentage of {111} facets. This result indicates that the photocatalytic activity increases with increasing surface area of the oxidation sites. In other word, the photocatalytic CO_2 reduction strongly depends on the rate of oxidative reaction or the consuming of the photogenerated hole on the TiO_2 surface by H_2O.

We also observed that brookite B_{Lys} showed a great improvement (1.3 times higher) in the photocatalytic CO_2 reduction compared to that of conventional brookite particles. This enhancement may be attributed to its well-grown exposed facets (Fig. 4e). The brookite nanocrystals are bound by {210}, {111}, and {110} facets. These facets induce the effective suppression of recombination rates of photogenerated electrons and holes by providing separated oxidative and reductive sites.[36–38] Such exposed facets have been found to be beneficial to the photoreduction of CO_2.[39,40]

3.5. Effect of co-catalyst loading

In order to enhance the quantum yield and selectivity from CO_2 reduction, a co-catalyst was used as the reductive sites and improve multi-electron reduction.[41–43] In this work, Pt was used as the co-catalyst, which plays a role as an electron trap to prevent the electron–hole combination. Fig. 9 shows TEM images of a Pt/TiO_2 rutile nanocrystals indicating the deposition of Pt nanoparticles of ~1 nm in size on the surface of TiO_2. Fig. 10 shows methanol yields on rutile and brookite with a Pt loading in comparison with samples without loading. The increase in methanol yield on Pt/TiO_2 was presumably due to the suppression of the electron–hole recombination. The photogenerated electron will be trapped at the Pt islands followed by the multi-electron reduction of CO_2.

3.6. Under visible light irradiation

We tested the photocatalytic activity of all the synthesized TiO_2 catalysts upon visible light ($\lambda > 400$ nm) irradiation.[24] However, only a small amount of methanol (less than 1 μmol g^{-1}) was detected, as shown in Fig. S7.†

4. Conclusions

In summary, well-defined titania nanostructures have been synthesized by a facile hydrothermal method with amino acids as the shape-controlling agent. The titania phases of anatase, rutile or brookite can be easily tuned by using different kinds of amino acid. High aspect ratio rod-like rutile has been synthesized by using a glutamic acid additive. Brookite with a small size and well-faceted surface can be obtained in the presence of lysine. Amino acids play versatile roles as pH-adjusting and capping agents for controlling the crystalline structure, size and shape of the synthesized nanoparticles. Among the rutile samples, the photocatalytic activity increases with increasing {111} surface percentage. Brookite with exposed {210} facets exhibited a notable photocatalytic reduction of CO_2 to methanol, presumably due to its specific surface structure with spatial separation of the reductive and oxidative sites. Our studies demonstrate the abilities of size-control and facet-selectivity in determining photocatalytic activity, representing a critical step forward in the designing of high performance nanostructures for the photocatalytic reduction of CO_2 to methanol.

Acknowledgements

The authors wish to thank Professor Masato Kakihana at Tohoku University for fruitful discussion. This work was partly supported by a Grant-in-Aid for Basic Research from the Vietnam National University.

References

1 T. Inoue, A. Fujishima, S. Konishi and K. Honda, *Nature*, 1979, 277, 637–638.
2 J. Mao, K. Li and T. Y. Peng, *Catal. Sci. Technol.*, 2013, 3, 2481–2498.
3 Y. Ma, X. Wang, Y. Jia, X. Chen, H. Han and C. Li, *Chem. Rev.*, 2014, **114**, 9987–10043.
4 M. Asadi, B. Kumar, A. Behranginia, B. A. Rosen, A. Baskin, N. Repnin, D. Pisasale, P. Phillips, W. Zhu and R. Haasch, *Nat. Commun.*, 2014, **5**, 4470.

5 F. Studt, I. Sharafutdinov, F. Abild-Pedersen, C. F. Elkjær, J. S. Hummelshøj, S. Dahl, I. Chorkendorff and J. K. Nørskov, *Nat. Chem.*, 2014, **6**, 320–324.
6 R. Kuriki, K. Sekizawa, O. Ishitani and K. Maeda, *Angew. Chem., Int. Ed.*, 2015, **54**, 2406–2409.
7 D. Kim, J. Resasco, Y. Yu, A. M. Asiri and P. Yang, *Nat. Commun.*, 2014, **5**, 4948.
8 S. Kattel, P. J. Ramírez, J. G. Chen, J. A. Rodriguez and P. Liu, *Science*, 2017, **355**, 1296–1299.
9 P. Gao, S. Li, X. Bu, S. Dang, Z. Liu, H. Wang, L. Zhong, M. Qiu, C. Yang, J. Cai, W. Wei and Y. Sun, *Nat. Chem.*, 2017, DOI: 10.1038/nchem.2794.
10 J. Graciani, K. Mudiyanselage, F. Xu, A. E. Baber, J. Evans, S. D. Senanayake, D. J. Stacchiola, P. Liu, J. Hrbek, J. F. Sanz and J. A. Rodriguez, *Science*, 2014, **345**, 546–550.
11 L. Liu, Y. Jiang, H. Zhao, J. Chen, J. Cheng, K. Yang and Y. Li, *ACS Catal.*, 2016, **6**, 1097–1108.
12 J. Yu, J. Low, W. Xiao, P. Zhou and M. Jaroniec, *J. Am. Chem. Soc.*, 2014, **136**, 8839–8842.
13 S. Chatman, P. Zarzycki and K. M. Rosso, *ACS Appl. Mater. Interfaces*, 2015, **7**, 1550–1559.
14 S. N. Habisreutinger, L. Schmidt-Mende and J. K. Stolarczyk, *Angew. Chem., Int. Ed.*, 2013, **52**, 7372–7408.
15 Z. He, L. Wen, D. Wang, Y. Xue, Q. Lu, C. Wu, J. Chen and S. Song, *Energy Fuels*, 2014, **28**, 3982–3993.
16 K. Tomita, V. Petrykin, M. Kobayashi, M. Shiro, M. Yoshimura and M. Kakihana, *Angew. Chem., Int. Ed.*, 2006, **45**, 2378–2381.
17 Q. D. Truong, L. X. Dien, D.-V. N. Vo and T. S. Le, *J. Solid State Chem.*, 2017, **251**, 143–163.
18 M. Kobayashi, V. Petrykin, M. Kakihana and K. Tomita, *J. Am. Ceram. Soc.*, 2009, **92**, 21–26.
19 Y. Ohno, K. Tomita, Y. Komatsubara, T. Taniguchi, K. Katsumata, N. Matsushita, T. Kogure and K. Okada, *Cryst. Growth Des.*, 2011, **11**, 4831–4836.
20 Q. D. Truong, M. Kobayashi, H. Kato and M. Kakihana, *J. Cryst. Growth*, 2015, **418**, 86–91; Q. D. Truong, H. T. Hoa and T. S. Le, *J. Colloid Interface Sci.*, 2017, **504**, 223–229.
21 K. Kanie and T. Sugimoto, *Chem. Commun.*, 2004, 1584–1585; O. Durupthy, J. Bill and F. Aldinger, *Cryst. Growth Des.*, 2007, **7**, 2696–2704.
22 Y. Pan, W. Lv, Y. Niu, K. Wen, X. Hou, J. Gu, M. Zou, L. Ye, W. Wang, K. H. L. Zhang and W. He, *RSC Adv.*, 2015, **5**, 54605–54612; W. Lv, W. Huo, Y. Niu, Y. Zhu, Y. Xie, X. Guo and W. He, *CrystEngComm*, 2015, **17**, 729–733; W. Lv, X. Yang, W. Wang, Y. Niu, Z. Liu and W. He, *ChemPhysChem*, 2014, **15**, 2688–2691; M. Sushko and K. Rosso, *Nanoscale*, 2016, **8**, 19714–19725; X. Zhang, Y. He, M. L. Sushko, J. Liu, L. Luo, J. J. De Yoreo, S. X. Mao, C. Wang and K. M. Rosso, *Science*, 2017, **356**, 434–437.
23 Q. D. Truong, J. Y. Liu, C. C. Chung and Y. C. Ling, *Catal. Commun.*, 2012, **19**, 85–89.
24 Q. D. Truong, T. H. Le, J. Y. Liu, C. C. Chung and Y. C. Ling, *Appl. Catal., A*, 2012, **437–438**, 28–35.
25 T. V. Nguyen and J. C. S. Wu, *Appl. Catal., A*, 2008, **335**, 112–120.
26 I.-H. Tseng, W.-C. Chang and J. C. S. Wu, *Appl. Catal., B*, 2002, **37**, 37–48.
27 H. Z. Zhang and J. F. Banfield, *J. Phys. Chem. B*, 2000, **104**, 3481–3487.
28 G. A. Tompsett, G. A. Bowmaker, R. P. Cooney, J. B. Metson, K. A. Rodgers and J. M. Seakins, *J. Raman Spectrosc.*, 1995, **26**, 57–62.
29 M. Kobayashi, V. Petrykin, K. Tomita and M. Kakihana, *J. Cryst. Growth*, 2011, **337**, 30–37.
30 T. A. Kandiel, A. Feldhoff, L. Robben, R. Dillert and D. W. Bahnemann, *Chem. Mater.*, 2010, **22**, 2050–2060.
31 L. J. Liu, H. L. Zhao, J. M. Andino and Y. Li, *ACS Catal.*, 2012, **2**, 1817–1828.
32 T. Ohno, K. Sarukawa and M. Matsumura, *New J. Chem.*, 2002, **26**, 1167–1170.
33 E. Bae, N. Murakami and T. Ohno, *J. Mol. Catal. A: Chem.*, 2009, **300**, 72–79.
34 N. Murakami, Y. Kurihara, T. Tsubota and T. Ohno, *J. Phys. Chem. C*, 2009, **113**, 3062–3069.
35 N. Murakami, S. Katayama, M. Nakamura, T. Tsubota and T. Ohno, *J. Phys. Chem. C*, 2011, **115**, 419–424.
36 H. F. Lin, L. P. Li, M. L. Zhao, X. S. Huang, X. M. Chen, G. S. Li and R. C. Yu, *J. Am. Chem. Soc.*, 2012, **134**, 8328–8331.
37 M. Zhao, H. Xu, H. Chen, S. Ouyang, N. Umezawa, D. Wang and J. Ye, *J. Mater. Chem. A*, 2015, **3**, 2331–2337.
38 M. Zhao, H. Xu, H. Chen, S. Ouyang, N. Umezawa, D. Wang and J. Ye, *J. Mater. Chem. A*, 2015, **3**, 2331–2337.
39 T. Ohno, T. Higo, N. Murakami, H. Saito, Q. Zhang, Y. Yang and T. Tsubota, *Appl. Catal., B*, 2014, **152**, 309–316.
40 K. Li, B. Peng, J. Jin, L. Zan and T. Peng, *Appl. Catal., B*, 2017, **203**, 910–916.
41 W. N. Wang, W. J. An, B. Ramalingam, S. Mukherjee, D. M. Niedzwiedzki, S. Gangopadhyay and P. Biswas, *J. Am. Chem. Soc.*, 2012, **134**, 11276–11281.
42 W. B. Hou, W. H. Hung, P. Pavaskar, A. Goeppert, M. Aykol and S. B. Cronin, *ACS Catal.*, 2011, **1**, 929–936.
43 J. Mao, L. Ye, K. Li, X. Zhang, J. Jiu, T. Peng and L. Zan, *Appl. Catal., B*, 2014, **144**, 855–862.